A Kinetic, Spectroscopic, and Redox Study of Human Tryptophan 2,3-Dioxygenase[†]

Jaswir Basran,[‡] Sara A. Rafice,[§] Nishma Chauhan,[§] Igor Efimov,[§] Myles R. Cheesman,[||] Lila Ghamsari,[‡] and Emma Lloyd Raven*[,‡]

Department of Biochemistry, Henry Wellcome Building, University of Leicester, University Road, Leicester LE1 7RH, England, Department of Chemistry, University of Leicester, Lancaster Road, Leicester LE1 9HN, England, and School of Chemical Sciences and Pharmacy, University of East Anglia, Norwich NR4 7TJ, England

Received December 8, 2007; Revised Manuscript Received February 7, 2008

ABSTRACT: The family of heme dioxygenases, as exemplified by indoleamine 2,3-dioxygenase and tryptophan 2,3-dioxygenase, catalyzes the oxidative cleavage of L-tryptophan to *N*-formylkynurenine. Here, we describe a bacterial expression system for human tryptophan 2,3-dioxygenase (rhTDO) together with spectroscopic, kinetic, and redox analyses. We find unexpected differences between human tryptophan 2,3-dioxygenase and human indoleamine 2,3-dioxygenase [Chauhan et al. (2008) *Biochemistry 47*, 4761−4769]. Thus, in contrast to indoleamine 2,3-dioxygenase, the catalytic ferrous−oxy complex of rhTDO is not observed, nor does the enzyme discriminate against substrate binding to the ferric derivative. In addition, we show that the rhTDO is also catalytically active in the ferric form. These new findings illustrate that significant mechanistic differences exist across the heme dioxygenase family, and the data are discussed within this broader framework.

The L-kynurenine pathway, which leads to the formation of NAD, is the major catabolic route of L-tryptophan metabolism in biology. The initial step in this pathway is oxidation of L-tryptophan to *N*-formylkynurenine (Scheme 1). In all biological systems examined to date, this is catalyzed by one of two heme enzymes, tryptophan 2,3-dioxygenase (TDO)[1] or indoleamine 2,3-dioxygenase (IDO), in a reaction mechanism that involves binding of O_2 to ferrous heme.

In mammalian systems, IDO is ubiquitously distributed but is not found in the liver; tryptophan 2,3-dioxygenase, on the other hand, is found exclusively in the liver (*1*). For the mammalian enzymes, the best information that is available so far is for human IDO. In this case, new expression systems (*2*–*4*) have allowed the first functional information to emerge. More recently, a crystal structure for human IDO has been published (*5*).

In this paper, we report an expression system for recombinant human TDO and describe spectroscopic, kinetic, and redox analyses on the purified protein. We find unexpected differences between human TDO and human IDO (*6*) in terms of both substrate binding and the catalytic reaction intermediates. These new data considerably widen the scope of information available on the heme dioxygenase enzymes, and we use it to make functional comparisons both with human IDO and more generally across the heme dioxygenase family.

Scheme 1: Reaction Catalyzed by TDO, with IUPAC Numbering Indicated

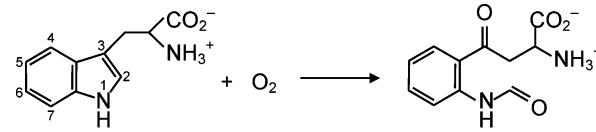

EXPERIMENTAL PROCEDURES

Materials. L-Ascorbate, bovine liver catalase, DNase I, D-glucose, glucose oxidase, methylene blue, nile blue chloride, xanthine, xanthine oxidase, L-tryptophan, and substrate analogues were purchased from Sigma-Aldrich Co. Restriction enzymes and DNA-modifying enzymes were from MBI fermentas. *Escherichia coli* strain BL21(DE3) pLysS was from Novagen. Hemin was obtained from Fluka.

Cloning and Expression of Recombinant Human TDO. The gene encoding human TDO was isolated by PCR amplification from a cDNA clone (IMAGE clone ID 4071714) obtained from a human liver cDNA library. The primers 5′ GCC TTT TCA CCA TGG CGG GGT GCC CAT TTT TAG G 3′ (forward primer) and 5′ CAT AGA TTT TGC AGA CGC TCG AGA TCT GAT TCA TCA C 3′ (reverse primer) were designed with reference to the published

[†] This work was supported by grants from BBSRC (project grants BB/C00602X/1 and IIP0206/009), EPSRC (studentships to S.R. and N.C.), and The Leverhulme Trust (fellowship to E.L.R.).

* To whom correspondence should be addressed. Telephone: +44 (0)116 229 7047. Fax: +44 (0)116 252 3789. E-mail: emma.raven@le.ac.uk.

[‡] Department of Biochemistry, University of Leicester.

[§] Department of Chemistry, University of Leicester.

[||] School of Chemical Sciences and Pharmacy, University of East Anglia.

[1] Abbreviations: TDO, tryptophan 2,3-dioxygenase; rhTDO, recombinant human tryptophan 2,3-dioxygenase; xTDO, *Xanthomonas campestris* tryptophan 2,3-dioxygenase; IDO, indoleamine 2,3-dioxygenase; rhIDO, recombinant human indoleamine 2,3-dioxygenase; L-Trp, L-tryptophan.

10.1021/bi702393b CCC: $40.75
Published on Web 03/28/2008

sequence of the gene encoding TDO (GenBank number BC005355) and incorporated 5′ *Nco*I and 3′ *Xho*I restriction sites (underlined). The *Nco*I−*Xho*I PCR fragment was cloned into pET28a (Novagen) to produce plasmid pEThTDO8, which encodes a C-terminal hexahistidine fusion of TDO cleavable with thrombin. DNA sequencing (Protein and Nucleic Acid Laboratory, University of Leicester) confirmed that no spurious mutations had arisen during the PCR.

For expression of recombinant human TDO (rhTDO), transformed cells of *E. coli* strain BL21(DE3)pLysS harboring the pEThTDO8 expression plasmid were grown overnight at 37 °C in LB media supplemented with 30 μg/mL kanamycin. The overnight culture (10 mL) was used to inoculate 0.5 L of 2× YT media containing 30 μg/mL kanamycin. The cultures were grown at 37 °C until the optical density at 600 nm reached a value of ∼0.8, and then isopropyl 1-thio-β-D-galactopyranoside (to a final concentration of 0.2 mM) and 0.5 mL of 3 mM hemin (in 10 mM NaOH) were added. The temperature was reduced to 25.0 °C and the incubation continued overnight. Cells were harvested by centrifugation (15 min, 6000 rpm, 4 °C) and stored at −80 °C.

Protein Purification and Handling. Cell pellets were resuspended in lysis buffer (50 mM NaH_2PO_4, 300 mM NaCl, 10 mM imidazole, pH 8.0) supplemented with two Complete protease inhibitor tablets (Roche) and lysed by the addition of 5 mg of lysozyme and by sonication (6 × 30 s pulses with 30 s intervals using a MSE Soniprep 150 sonicator). After sonication, DNase I was added and the suspension stirred for 30 min at 4 °C. The lysate was centrifuged at 18000 rpm for 50 min, and the cell-free extract loaded onto a 20 mL column of Ni-NTA Superflow resin (Qiagen) equilibrated in lysis buffer. The resin was washed with 300 mL of wash buffer (50 mM NaH_2PO_4, 300 mM NaCl, 20 mM imidazole, pH 8.0), and the protein was eluted using a linear gradient ranging from 20 to 250 mM imidazole in 50 mM NaH_2PO_4 and 300 mM NaCl, pH 8.0. TDO-containing fractions were pooled and dialyzed against 50 mM Tris-HCl buffer, pH 8.0, and frozen in aliquots at −80 °C.

Reconstitution of TDO. rhTDO isolated from *E. coli* exists as a mixture of apo- and holoenzyme forms. For this reason rhTDO was reconstituted with hemin prior to use in biochemical studies. rhTDO (typically 100 μM) was mixed with 1.5 equiv of hemin and incubated on ice in the dark for 1–2 h. Free hemin was removed from the protein by passage through a small gel filtration (Bio-Rad 10 DG) column and the eluant concentrated using a Centricon YM-30 (30 kDa) filtration unit. An absorption coefficient of $\epsilon_{408} = 196\ mM^{-1}\ cm^{-1}$ was determined for ferric rhTDO using the pyridine−hemochromagen procedure (*7*).

Steady-State Kinetic Assays. TDO activity was measured by monitoring the formation of *N*-formylkynurenine at 321 nm. Steady-state kinetic measurements were carried out using a Varian Cary 50 probe UV–visible spectrophotometer with a 1 cm light path. Reactions were performed at 25.0 °C in 50 mM Tris-HCl buffer, pH 8.0, containing 10 μM methylene blue, 100 μg of catalase, 20 mM L-ascorbate, and a fixed concentration of rhTDO. The reaction was initiated by the addition of tryptophan (or tryptophan analogue), and initial rates were calculated from the absorbance increase at 321 nm [$\epsilon_{321} = 3750\ M^{-1}\ cm^{-1}$ (*2*)]. Apparent K_M and k_{cat} values were determined by varying the concentration of each substrate and fitting the data to the Michaelis–Menten equation using the Grafit software package (*8*).

Electronic Spectroscopy. All absorbance spectra and equilibrium ligand binding experiments were measured in 50 mM Tris-HCl buffer, pH 8.0, at 25.0 °C using a Varian Cary 50 probe UV–visible spectrophotometer. Ferrous rhTDO was generated by stoichiometric titration of the ferric enzyme with sodium dithionite. The ferrous−oxy and ferrous−CO derivatives were generated by direct bubbling of O_2 and CO gases, respectively, through dithionite-reduced samples. Absorption spectra for rhTDO ferric−azide, ferric−fluoride, and ferrous−cyanide complexes were recorded in the presence of 5 M, 1 M, and 15 mM ligand, respectively.

Equilibrium binding constants, K_D, for binding of various ligands to ferric and ferrous forms of rhTDO were determined according to published procedures (*9*) and typically involved the addition of small volumes (0.5−2.0 μL) of ligand (from an appropriate stock solution) to the protein (∼1–5 μM) until no further spectral change occurred. Binding constants were determined spectrophotometrically by monitoring the change in absorbance at the appropriate wavelength and fitting to eq 1:

$$\Delta Abs = (K_D A_i + [L]_{tot} A_f)/(K_D + [L]_{tot}) \quad (1)$$

where A_i and A_f are the initial and final absorbance values, respectively, and $[L]_{tot}$ is the total concentration of the ligand. The binding of CO to the ferrous enzyme in the presence (4 mM) and absence of L-Trp was followed at 421 nm; the K_D for CO binding to the ferrous−Trp complex was calculated using eq 2, which was used instead of eq 1 because of the tighter binding affinity:

$$\Delta A = \frac{\Delta A_\infty}{2[E]}[E + L + K_d - \{(E + L + K_d)^2 - 4[E][L]\}^{1/2}] \quad (2)$$

where [E] and [L] represent the calculated concentrations of total enzyme and total ligand, respectively, after each addition and ΔA and ΔA_∞ are the absorbance changes corresponding to intermediate and saturating ligand concentrations. Binding constants were also determined kinetically, using stopped flow (*vide infra*).

EPR Spectroscopy. EPR spectra were recorded using a Bruker ER300D spectrometer fitted with a dual-mode cavity, type ER4116M, interfaced to an ELEXYS computer control system (Bruker Analytische Messtechnik GmBH) and equipped with a variable temperature cryostat and liquid helium transfer line (Oxford Instruments). EPR simulations were performed using the Bruker program WINEPR Simfonia (v1.25). Determination of low-spin heme concentrations was achieved by simulation and double integration of spectra recorded under nonsaturating conditions at 15 K using 1 mM Cu(II)-EDTA as a spin standard. Enzyme samples were prepared in 50 mM potassium phosphate, pH 8.0. For samples in the presence of L-Trp, the substrate (10 mM stock solution in buffer) was added to a final concentration of 3 mM and then frozen immediately to prevent oxidation of the substrate. Final concentrations of enzyme were 60 μM in both cases.

Stopped-Flow Kinetics. Stopped-flow experiments were carried out using an Applied Photophysics SX.18 MV

Table 1: Absorption Maxima (nm) for rhTDO (50 mM Tris-HCl Buffer, pH 8.0, 25.0 °C)

derivative	rhTDO	rat liver[a]	*B. brevis*[b]	*P. fluorescens*[c]
ferric	408, 533, 621	406, 498, 632	407, 500, 630	405, 500, 635
ferric + L-Trp	410, 536, 565 sh[g]	407, 498, 632[d]		
ferrous	428, 533, 560	430, 557	432, 555, 585	432, 553, 588
ferrous + L-Trp	426, 533, 560	421, 557[d]		
ferrous−cyanide	430, 534, 564			
ferrous−oxy	413[e]			
ferrous−CO	421, 540, 564	420, 538, 569		
ferrous−CO + L-Trp	421, 540, 564	420, 538, 569		
ferric−azide	415, 540[f]			
ferric−cyanide	419, 538, 566 sh			
ferric−fluoride	406, 527, 633[f]			

[a] Taken from ref *15*. [b] Taken from ref *16*. Only the ferric and ferrous derivatives have been reported. [c] Taken from ref *14*. Only the ferric and ferrous derivatives have been reported. [d] Assumed (i.e., authors have stated there is no spectral change upon addition of substrate). [e] This derivative shows only a broad, featureless spectrum in the visible region, with no evidence of the characteristic oxy peaks. There is a broad peak with a maximum at ≈526 nm. [f] Binding of these ligands to rhTDO is substantially weaker than for cyanide, meaning that dissociation constants could not be calculated accurately for these complexes. [g] sh = shoulder.

stopped-flow spectrophotometer. Unless otherwise stated, measurements were carried out at 25.0 °C in 50 mM Tris-HCl buffer, pH 8.0. For experiments performed under anaerobic conditions, the sample-handling unit of the stopped-flow instrument was contained within a Belle Technology glovebox. Buffers were made anaerobic by bubbling oxygen-free nitrogen gas through solutions for ~2 h. Buffers were then placed in the glovebox overnight to remove any residual traces of oxygen. Solutions of dithionite and substrate were made by adding the appropriate solid to anaerobic buffer. Stopped-flow, multiple-wavelength absorption studies were carried out using a photodiode array detector and X-SCAN software (Applied Photophysics Ltd.). In single wavelength studies, changes in absorbance were monitored at 408 nm. Transients were either monophasic or biphasic and were fitted using the standard single or double exponential equations, respectively.

Mass Spectrometry. Protein bands of interest were excised from an SDS gel and subjected to in-gel trypsin digestion (*10*). Proteolytic peptide fragments were analyzed by MALDI-ToF mass spectrometry: the sample was mixed 1:1 with α-cyano-4-hydroxycinnamic acid (5 mg/mL in 0.1% TFA/50% acetonitrile), spotted onto a stainless steel MALDI target plate, and analyzed using a Voyager DE-STR MALDI-ToF mass spectrometer (Applied Biosystems). The resulting peptide masses were analyzed against the NCBInr protein database using the MASCOT search algorithm (Matrix Science, London, U.K.). A 95% significance threshold was used for validating statistically significant identifications.

Redox Potentiometry. Reduction potentials for Fe^{3+}/Fe^{2+} of rhTDO were determined by the reduction of a dye with a known potential (*11*). The assay solution contained potassium phosphate buffer (0.1 M, pH 7.0), glucose (5 mM), xanthine (300 μM), xanthine oxidase (50 nM), glucose oxidase (50 μg/mL), catalase (5 μg/mL), enzyme (2 μM), and either the dye nile blue chloride [$E^{\circ\prime} = -116$ mV (*12*)] or the dye methylene blue [$E^{\circ\prime} = +11$ mV (*12*)]. The components glucose, glucose oxidase, and catalase generated an oxygen-free environment. The absorbance change for the heme peak was measured at the isosbestic point for the dye at 410 nm, and the absorbance change for the dye was measured at the isosbestic point for the heme peak at 635 nm using a Perkin-Elmer Lambda 40 spectrophotometer; at these wavelengths there is no absorption from the other components of the reaction solution.

The results were analyzed using the Nernst equations [25 mV $\ln(E_{ox}/E_{red})$] and [12.5 mV $\ln(D_{ox}/D_{red})$], where E_{ox}/E_{red} and D_{ox}/D_{red} are the oxidized and reduced forms of the enzyme and dye, respectively, thus producing a linear graph, with a slope of 1 across a wide potential range (*6*). Determination of the relationship between equilibrium binding constants for oxidized, K_{ox}, and reduced, K_{red}, proteins and the reduction potential was according to the thermodynamic cycle in eq 3:

$$K_{ox}/K_{red} = \exp[F(E^{bound} - E^{free})/RT] \quad (3)$$

where K_{ox} and K_{red} are equilibrium binding constants for oxidized and reduced rhTDO, respectively, E^{bound} and E^{free} are the redox potentials of rhTDO bound to L-tryptophan and free protein, respectively, R is the gas constant, F is the Faraday constant, and T is the temperature.

RESULTS

Protein Expression and Purification. Recombinant human TDO was expressed in *E. coli* as a full-length, C-terminal hexahistidine fusion protein. An expression system for rat TDO has been previously reported (*13*). Our expression system for rhTDO gave yields of purified protein of ≈15 mg/L. Trypsin digestion of a sample of enzyme followed by MALDI-ToF mass spectrometry gave clear indication that the protein band is indeed rhTDO (Supporting Information, Figure S1).

Electronic Spectroscopy. The absorption maxima for various ferric and ferrous derivatives of rhTDO are given in Table 1. Maxima for a few derivatives have been published for the rat liver enzyme and for the bacterial *Bacillus brevis* and *Pseudomonas fluorescens* enzymes (*14–16*);[2] these are compared with rhTDO in Table 1. The spectrum of the ferric form of rhTDO has maxima at 408, 533, and 621 nm (Table 1 and Figure 1A), consistent with there being a mixture of high- and low-spin heme species. As observed previously for human IDO (*3*), the binding of L-Trp to ferric rhTDO leads to a red shift of the Soret band (to 410 nm), increases in the low-spin signatures at 536 and 565 nm, and decreases

[2] For these other TDOs, there is very limited information available. The majority of the published information is summarized in Table 1, but k_{cat} and K_M values have also been reported, as discussed in the text below.

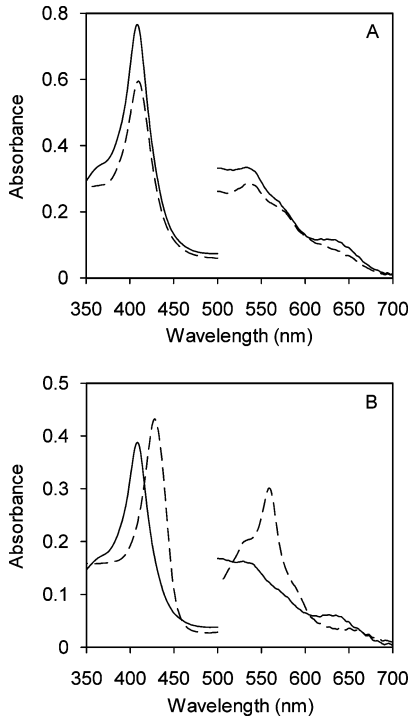

FIGURE 1: Electronic absorption spectra of rhTDO. (A) Ferric rhTDO in the absence (solid line) and presence (dashed line) of L-Trp. (B) Ferric rhTDO (solid line) and ferrous rhTDO (dashed line). Absorbance values in the visible region have been multiplied by a factor of 4. Reaction conditions: 50 mM Tris-HCl, pH 8.0, 25.0 °C.

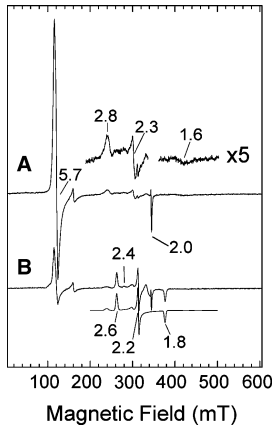

FIGURE 2: X-band EPR spectra of rhTDO in the absence (A) and presence (B) of L-Trp. Spectra were recorded at a temperature of 10 K using 2.01 mW microwave power at a frequency of 9.67 GHz and a modulation amplitude of 1 mT. Spectra are adjusted to account for differences in receiver gain. The trace below the experimental spectrum in (B) is a simulation of the contributions from two low-spin hemes with g_{zyx}-values and line widths (W_{zyx}) as follows: species a, 2.632, 2.202, 1.835 (4.1, 2.3, 3.6 mT); species b, 2.892, 2.297, 1.620 (8.0, 5.7, 20.0 mT).

in absorbance at 621 nm (Figure 1A), all of which are consistent with the formation of a low-spin heme species on addition of substrate.

Reduction of ferric rhTDO results in a red shift in the Soret band (from 408 to 428 nm) and the formation of a sharp peak in the visible region (560 nm) (Figure 1B).

EPR Spectroscopy. Figure 2A shows the low-temperature X-band EPR spectrum of rhTDO and is dominated by an axial spectrum ($g_{xy} = 5.71$, $g_z = 2.01$) typical of high-spin ferric heme. The presence of a minority low-spin form

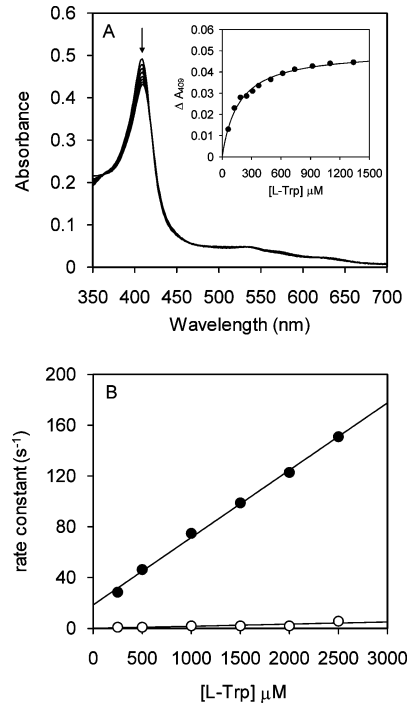

FIGURE 3: Reaction of ferric rhTDO (2.5 μM) with L-Trp. (A) Representative data set for the determination of K_D for binding of L-Trp to rhTDO. The arrow indicates the direction of change in absorbance upon successive additions of L-Trp. Inset: Absorbance change at 409 nm upon successive additions of L-Trp and fit of the data to eq 1. (B) Dependence of the rate constant on concentration for the fast (closed circles) and slow (open circles) phases of the biphasic reaction of rhTDO with substrate (monitored at 408 nm). Reaction conditions: 50 mM Tris-HCl, pH 8.0, 25.0 °C.

(species b) is evident ($g = 2.89$, 2.30, 1.62) and is shown in the expansion in Figure 2A. These high- and low-spin species correlate with those observed for rhIDO [$g = 5.82$, 1.99 and $g = 2.85$, 2.27, 1.62, respectively (*6*)], although there is a higher proportion of high-spin heme for ferric rhTDO than in the corresponding spectrum for rhIDO.

On addition of substrate (Figure 2B), there is a substantial decrease in the level of the high-spin species coupled with the emergence of a new low-spin form (species a) with *g*-values of 2.63, 2.20, 1.84. These *g*-values correspond with those previously observed for ferric rhIDO in the presence of L-Trp [$g = 2.52$, 2.19, 1.86 (*3*)] and have been assigned as arising from hydroxide-bound heme. A similar assignment is proposed here for rhTDO, which is in agreement with the UV–visible data presented above. Underneath the spectrum shown in Figure 2B is a simulation of the spectrum of both this new low-spin species a plus a residual amount of species b.

Binding of L-Trp to Ferric rhTDO. Absorbance changes observed upon binding of L-Trp to ferric rhTDO (under anaerobic conditions, Figure 3A) give a dissociation constant, K_D, of 170 ± 11 μM (Figure 3A, inset). The binding of L-Trp was also measured kinetically under pseudo-first-order conditions ([L-Trp] ≫ [rhTDO]). Absorption changes at 408 nm were biphasic with the first phase contributing the majority (60−70%) of the total amplitude change. The observed pseudo-first-order rate constant for the fast phase (k_{obs1}) was linearly dependent on L-Trp concentration (Figure 3B) and gives a slope ($=k_{on}$) of 0.053 ± 0.001 μM^{-1} s^{-1} and intercept ($=k_{off}$) of 18.5 ± 2 s^{-1}. The calculated K_D

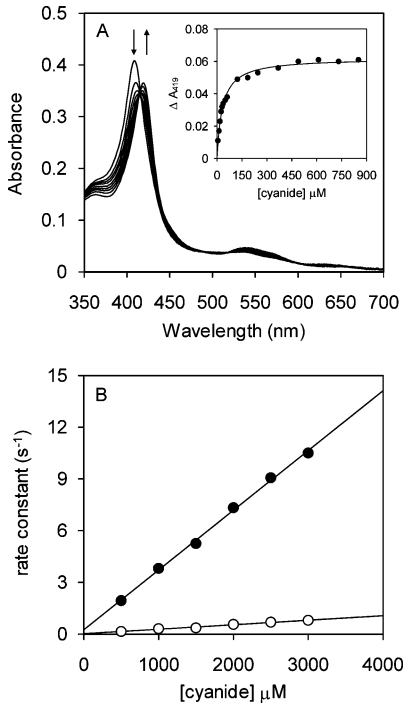

FIGURE 4: Reaction of ferric rhTDO (2.0 μM) with cyanide. (A) Representative data set for the determination of K_D for binding of cyanide to rhTDO. The arrows indicate the direction of changes in absorbance upon successive additions of cyanide. Inset: Absorbance change at 419 nm upon successive additions of cyanide and fit of the data to eq 1. (B) Dependence of the rate constant on concentration for the fast (closed circles) and slow (open circles) phases of the biphasic reaction of rhTDO with cyanide (monitored at 419 nm). Reaction conditions: 50 mM Tris-HCl, pH 8.0, 25.0 °C.

($=k_{off}/k_{on}$) is thus 349 ± 44 μM, similar to that obtained by equilibrium titration (*vide supra*). The observed rate constant for the second phase (k_{obs2}) was weakly dependent on L-Trp concentration (Figure 3B). We assign this biphasic behavior as arising from the existence of multiple heme conformers that are in slow equilibrium.

Binding of Cyanide to Ferric rhTDO. The equilibrium dissociation constant for the rhTDO−cyanide complex was calculated to be 33 ± 1.7 μM (Figure 4A and inset). In stopped-flow experiments, binding of cyanide to ferric rhTDO also occurred in two phases (as for L-Trp, above) with the first phase contributing ≈60% to the total absorption change. Each phase was linearly dependent on cyanide concentration with second-order rate constants of 0.0035 μM^{-1} s^{-1} and 0.0003 μM^{-1} s^{-1} for the fast and slow phases, respectively (Figure 4B). In this case, however, the intercepts are very close to zero and have large errors, making it difficult to calculate a K_D value with confidence.

Steady-State Oxidation of L- and D-Trp. Steady-state kinetic parameters for rhTDO with L-Trp and a number of substrate analogues (Scheme 2) are shown in Table 2. For comparison, data for rhIDO are also given. For rhTDO with L-Trp, k_{cat} = 1.4 ± 0.02 s^{-1} and K_M = 222 ± 15 μM. The steady-state turnover rate (k_{cat}) for both dioxygenases is the same (1.4 s^{-1}), although substrate binding for L-Trp is at least 20-fold weaker for rhTDO (K_M ≈ 220 μM compared with ≈10 μM for rhIDO). Similar values for k_{cat} and K_M have very recently been reported for a truncated form of rhTDO (*17*).

IDO from a number of different sources has been shown to be capable of catalytic turnover with the D-stereoisomer of Trp (*1, 18–20*). This is also true for the human enzyme (k_{cat} = 3.93 s^{-1}, Table 2), although the K_M value is >100-fold higher than for L-Trp, suggesting much weaker binding for D-Trp. For rhTDO, there is evidence for oxidation of D-Trp, but the activity is very low (Table 2). Given the relative binding affinities of the two enzymes for L-Trp (rhIDO > rhTDO) and of the two substrates for the two enzymes (L-Trp > D-Trp), this poor activity is probably a result of very weak binding of D-Trp to rhTDO.

Steady-State Oxidation of Other Trp Analogues. The heme dioxygenases can support insertion of O_2 into a number of ring-substituted tryptophan analogues. For rhIDO, substitutions at the 5-position of the indole ring (Scheme 1) are tolerated, and there is little effect on the affinity of these substituted analogues for the enzyme (Table 2). On the other hand, no detectable activity was observed with analogues in which either the amino group or the carboxylate group of the aliphatic side chain has been modified or is absent (Table 2).

For rhTDO, the only L-Trp analogues which could be oxidized were 5-fluoro-L-Trp and 5-methyl-L-Trp (although the latter very slowly, Table 2); all other derivatives tested gave no observable catalytic activity.

Oxidation of L-Trp by Ferric rhTDO. The steady-state assays above use ferrous rhTDO as the catalytically reactive form of the enzyme. However, we also observed activity with the ferric form of rhTDO. Incubation of ferric rhTDO with 2 mM L-Trp (50 mM Tris-HCl, pH 8.0) at atmospheric concentrations of O_2 results in an increase in absorption at 300–350 nm indicative of product formation (Figure 5A). In parallel experiments with ferric rhIDO under identical conditions, no increase in absorbance was observed on prolonged incubation (Figure 5B). When the experiments with rhTDO were repeated under anaerobic conditions, there was no significant increase in absorption at 321 nm (Figure 5C). The ratio of the absorbance changes measured at 321 nm was 150:7:1 for rhTDO (aerobic), rhTDO (anaerobic), and rhIDO, respectively, which gives an indication of the relative rates of the reactions. A truncated form of human TDO has also very recently been shown to have activity in the ferric form (*17*).

Binding of O_2 to Ferrous rhTDO. Bubbling of O_2 gas directly into a solution of ferrous rhTDO results in the formation of a species that has a Soret band at 413 nm, but there are no sharp peaks in the visible region (expected at ≈540 and ≈570 nm) that characterize this complex as a ferrous−oxy species (Table 1 and Figure 6A). To examine whether formation of a ferrous−oxy species was occurring over shorter time scales, the reaction was monitored using photodiode array spectroscopy (Figure 6B). In this experiment, data were collected over a period of 10 s from the mixing event. When mixed with O_2, ferrous rhTDO shows an overall decrease in absorbance in the visible region, and the Soret band decreases in intensity and is blue shifted (to 417 nm). There is no evidence for formation of the characteristic ferrous−oxy peaks (expected at ≈540 and ≈580 nm) even if the reaction is observed over an extended period (e.g., 200 s). The spectrum of the final species at 200 s is essentially identical to that obtained under equilibrium conditions when a solution of ferrous rhTDO was purged

Scheme 2: Structures of Tryptophan Derivatives Used in This Work

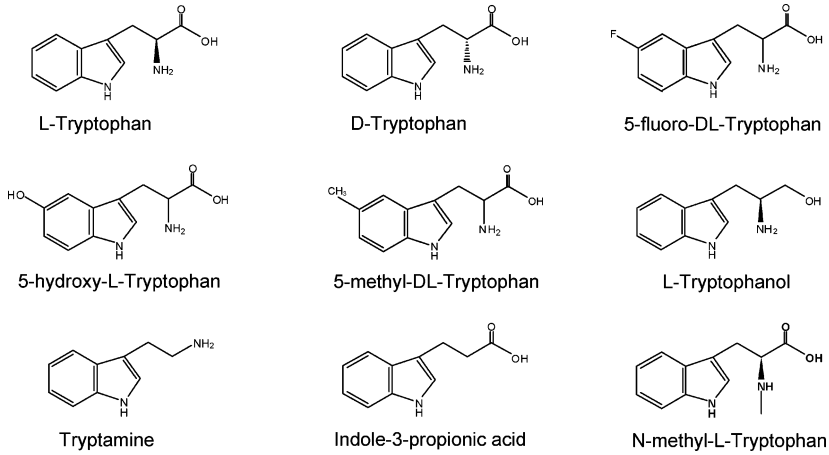

Table 2: Steady-State Parameters for Oxidation of L-Trp and Other Substrate Analogues by rhTDO and rhIDO (50 mM Tris-HCl Buffer, pH 8.0, 25.0 °C)

	rhIDO		rhTDO	
substrate	k_{cat} (s^{-1})	K_M (μM)	k_{cat} (s^{-1})	K_M (μM)
L-Trp	1.4 ± 0.05	7 ± 0.8	1.4 ± 0.019	222 ± 15
D-Trp	3.93 ± 0.07	1570 ± 100	*a*	*a*
5-fluoro-Trp	0.76 ± 0.01	6 ± 0.8	0.18 ± 0.004	360 ± 28
5-methyl-Trp	3.78 ± 0.16	98 ± 14	*b*	*b*
5-hydroxy-Trp	0.025 ± 0.0004	17 ± 1.1	no activity	
N-methyl-Trp	no activity		no activity	
tryptamine	no activity		no activity	
indole-3-propionic acid	no activity		no activity	
tryptophanol	no activity		no activity	

[a] Catalytic turnover of D-Trp was only measured at one concentration (50 mM) as very little activity was detectable at lower concentrations. At a concentration of 50 mM D-Trp, the measured rate of catalytic turnover for rhTDO was 0.073 s^{-1}, i.e., 5% of the k_{cat} value calculated for rhTDO with L-Trp. [b] In these assays the initial velocity was linearly dependent on 5-methyl-Trp concentration across the experimental range; the value of k_{cat}/K_M determined from the slope of this plot was 0.0001 μM^{-1} s^{-1}.

directly with O_2 gas (compare with Figure 6). By means of comparison, reaction of rhIDO with O_2 on the stopped-flow time scale leads to clear formation of a ferrous−oxy species (λ_{max} = 416, 539, and 576 nm), and this species is stable (*6*).

Binding of Other Ligands to Ferrous rhTDO. In contrast to the reaction with O_2, the ferrous−CO complex of rhTDO is readily isolated (λ_{max} = 421, 540 and 564 nm; Table 1 and Figure 6A). Addition of L-Trp (1 mM) to the ferrous−CO complex did not result in any further spectral change (Table 1). Binding constants, K_D, for binding of CO to ferrous rhTDO and the [ferrous rhTDO−Trp] complex were 5.1 ± 0.3 and 1.4 ± 0.15 μM, respectively. In addition, ferrous rhTDO also binds cyanide, as evidenced by the formation of sharp peaks at 534 and 564 nm in the visible region (Figure 6A).

Redox Potentiometry. Reduction potentials for the Fe^{3+}/Fe^{2+} couple of rhTDO in the absence, E^{free}, and presence, E^{bound}, of L-Trp were found to be −92 ± 3 and −76 ± 3 mV, respectively (Figure 7). This similarity in the two values was unexpected since in other heme dioxygenases a shift in reduction potential is observed on binding of substrate (*3, 21*). In separate experiments (data not shown), these reduction potentials were confirmed using methylene blue instead of nile blue chloride as the redox dye. As an independent check on whether the values were correct, these reduction potentials (E^{bound} = −76 mV and E^{free} = −92 mV) were correlated with the binding constants determined above for binding of L-Trp to the oxidized (K_{ox} = 170 μM) and reduced (K_{red} = 222 μM) states[3] according to eq 3 (where RT/F = 25 mV). In this case, a value for K_{ox}/K_{red} of 0.77 is calculated, which is similar to the value of 1.89 calculated for $\exp[F(E^{bound} - E^{free})/RT]$. The fact that these reduction potentials correlate with the experimentally determined values for the binding constants in this way is evidence that the measured reduction potentials in the absence and presence of substrate are indeed correct and are a true reflection of the binding thermodynamics.

DISCUSSION

In this work, we report a bacterial expression system for human TDO that produces milligram quantities of enzyme. This has allowed us to report detailed mechanistic and redox information for this human enzyme.[4] Below, we compare the properties of human TDO with other dioxygenase enzymes and discuss the implications of these data in terms of our current understanding of the heme dioxygenase structure and function.

Redox Properties. The Fe^{3+}/Fe^{2+} reduction potential for human TDO has not been reported previously and was determined here as −92 mV, which is in a similar range to that for rhIDO (*6*). There is no reliable determination of a

[3] In this treatment, we have assumed that $K_D \approx K_M$ for the reduced form.

[4] rhTDO is available commercially (www.genwaybio.com), although there are no functional data.

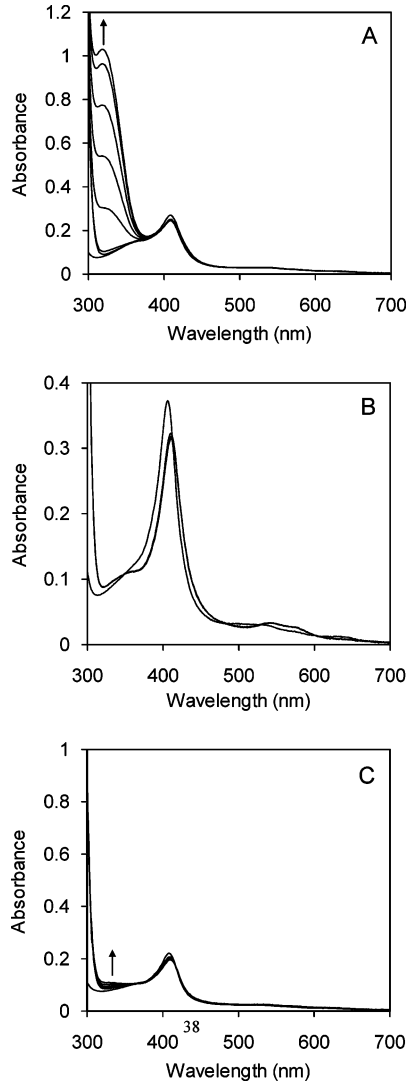

FIGURE 5: Oxidation of L-Trp by ferric rhTDO. (A) Spectral changes observed upon reaction of ferric rhTDO with L-Trp under aerobic conditions. (B) Spectral changes observed upon reaction of ferric rhIDO with L-Trp under aerobic conditions. (C) Spectral changes observed upon reaction of ferric rhTDO with L-Trp under anaerobic conditions. All reactions were monitored for 60 min; arrows indicate the direction of the absorbance change during the course of the reaction. Reaction conditions: 50 mM Tris-HCl, pH 8.0, 25.0 °C.

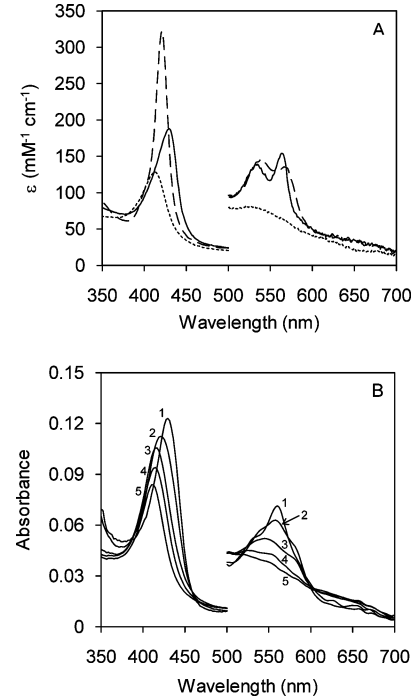

FIGURE 6: Electronic absorption spectra of ferrous derivatives of rhTDO. (A) UV–visible spectra of the ferrous complex in the presence of O_2 (dotted line), CO (dashed line), and CN (solid line) forms of rhTDO; absorbance values in the visible region have been multiplied by a factor of 4. (B) Reaction of rhTDO with O_2 monitored by stopped-flow photodiode array spectroscopy. Time-dependent spectral changes on mixing rhTDO with O_2 (time base of 10 s). For clarity, only selected spectra are shown at (1) 1.28 ms, (2) 100 ms, (3) 1 s, and (4) 10 s after mixing. The spectrum collected 200 s after mixing (5) is also shown. Reaction conditions: 50 mM Tris-HCl, pH 8.0, 25.0 °C.

reduction potential for a mammalian TDO.[5] The reduction potential for rhTDO does not shift significantly on addition of substrate. This has functional implications, since the reduction potentials of the substrate-bound and substrate-free forms of the enzyme report indirectly on the relative binding affinity of the substrate. Thus, with rhTDO the redox data show that there is no stabilization of the ferrous derivative upon binding of the substrate. This is in contrast to rhIDO and *Xanthomonas campestris* TDO in which the Fe^{3+}/Fe^{2+} reduction potentials increase by ≈60–80 mV (*3, 6*) and ≈140 mV (*21*), respectively, upon binding of L-Trp. The functional implications of this are discussed in more detail below.

Substrate Binding. Our data with the various substrate analogues clearly show that modifications to the α-carboxylate and/or α-ammonium groups of the substrate are not tolerated, which indicates that hydrogen-bonding interactions to these charged groups are important in the substrate-bound complex, as observed in the crystal structure of xTDO in complex with L-Trp (*21*).[6] An assessment of other TDOs for which binding of substrate analogues has been reported (Table 3) describes a similar picture, which suggests that binding interactions to the substrate across the TDO family are likely to be conserved.

The binding affinity of the substrate to ferric and ferrous rhTDO is in the same range as that to ferric rhIDO [≈200–300 μM in all cases (*6*)]. In human IDO, however, the substrate discriminates between the ferric and ferrous forms of the enzyme by a factor of ≈40 (*3*), so that the substrate binds preferentially to the ferrous form ($K_M \approx 10$ μM). As dictated by the reduction potentials (above), human

[5] The literature is confusing here. An early report (*22*) cites a value of −110 mV for rat liver TDO at pH 7 taken from ref *23* (which is cited as 1980b in ref *22*), but this value of −110 mV is not correct since in ref *23* no actual reduction potential is stated nor do the data that are shown indicate a potential close to this value. In ref *22* two papers by Makino et al. are cited (1980a and 1980b), and we assume that ref *22* incorrectly cites 1980b instead of 1980a. The correct 1980a reference (*24*) does give a reduction potential and the data are shown: a value of +100 mV is reported here in the absence of L-Trp, which shifts to +160 mV on addition of saturating concentrations of L-Trp.

[6] Binding of D-Trp is clearly much less favorable than that for L-Trp (Table 2). Batabyal et al. (*17*), however, report similar values of K_M for the two substrates in a truncated human TDO. We believe that this might arise from the fact that substrate is present during protein purification in ref *17* (which is not the case in our protein preparations) and that L-Trp might therefore be present in the D-Trp assays.

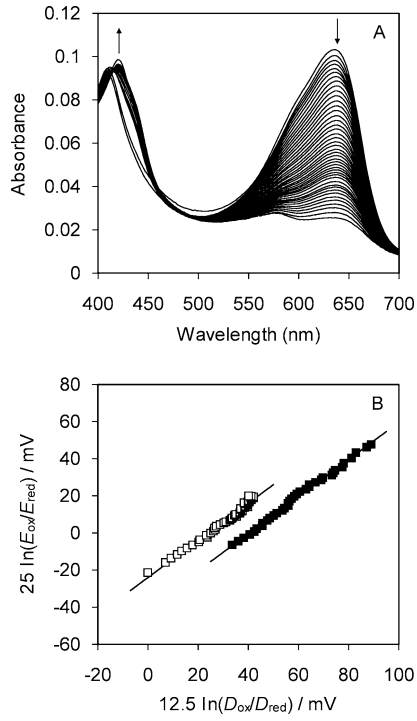

FIGURE 7: Redox potentiometry of rhTDO. (A) Spectral changes observed during determination of Fe^{3+}/Fe^{2+} reduction potential for rhTDO with the dye nile blue chloride. For clarity, only certain spectra are shown; arrows indicate the direction of absorption change during the reductive titration. (B) Nernst plots for the data shown in (A) (open squares) and for the data collected in the presence of substrate (filled squares). Reaction conditions: 100 mM potassium phosphate, pH 7.0, 25.0 °C.

Table 3: Activity of TDOs with Different Substrate Analogues[a]

	X. campestris[b]	*B. brevis*[c,d]	*S. parvulus*[e]	*R. metallidurans*[f]	mouse liver[g,h]
D-Trp	−	−	+	−	+
5-fluoro-Trp	+	+	+	nd	nd
5-OH-Trp	nd	+	nd	nd	−
5-methyl	nd	+	+	nd	nd
6-fluoro-Trp	+	+	nd	nd	nd
6-methyl	nd	+	nd	nd	nd
α-methyl	nd	nd	+	nd	nd
tryptamine	−	−	nd	−	−
serotonin	nd	nd	nd	nd	−
indolepropionic acid	−	−	nd	−	nd
indole	nd	−	nd	−	nd

[a] +, activity observed; −, no activity; nd, not determined. [b] Reference *21*. [c] Reference *15*. [d] Measured at 10 mM concentration of each substrate. [e] Reference *25*. [f] Reference *26*. [g] Reference *20*. [h] Authors demonstrate that rat liver TDO is also active with D-Trp.

TDO shows no such discrimination because in this case $K_{d(ferric)} \approx K_{M(ferrous)} \approx 200\ \mu M$.

Why then does IDO need to specifically favor substrate binding to the ferrous form whereas TDO does not? One explanation relates to the physiological location of the two dioxygenases. IDO is always located in the cytoplasm, which is an overall reducing environment. This would mean that only low concentrations of ferric IDO were present so that efficient binding to the ferric enzyme was not necessary *in vivo* (and consequently that the ferrous form binds substrate preferentially). On the other hand, human TDO is located exclusively in the liver, which is a more oxygen-rich (oxidizing) environment: this would mean that significant amounts of ferric TDO are present physiologically such that binding to the ferric protein needs to be more efficient relative to IDO.

Oxidation of Substrate. The value of k_{cat} for rhTDO is identical to that for rhIDO (1.4 s^{-1}). These values for the two mammalian enzymes are lower than those found typically for the bacterial enzymes [k_{cat} usually ≈20 s^{-1} (*14, 21, 23*)], although the reason for this difference is not clear at this stage. Most significantly for rhTDO, our data clearly show that oxidation of substrate is not a reaction catalyzed exclusively by the ferrous enzyme since substrate oxidation also occurs (albeit more slowly) with ferric rhTDO under aerobic conditions. Substrate oxidation by ferric rhTDO is most likely a result of trace amounts of either H_2O_2 and/or superoxide in solution. This is supported by the fact that substrate oxidation does not occur in the absence of O_2 and by separate experiments in which incubation of the reaction mix with either catalase or superoxide dismutase resulted in a 90% reduction in the total amount of product formed (data not shown). This characteristic ability of ferric rhTDO to catalyze product formation is not one that rhIDO can duplicate. The difference most likely relates to the fact that rhIDO discriminates against substrate binding to the ferric enzyme ($K_{M(ferrous)} \ll K_{d(ferric)}$, as discussed above) whereas TDO does not and the fact that higher concentrations of ferric enzyme are likely present *in vivo* for TDO.

Formation of the Catalytic Ferrous−Oxy Complex. In our experiments under equilibrium and pre-steady-state conditions we find no evidence for formation of a stable ferrous–oxy complex of rhTDO. This inability of rhTDO to binding O_2 does not derive from an intrinsically unreactive ferrous heme group, since reaction of ferrous rhTDO with other diatomics (cyanide, CO) occurs normally. Our complete failure to detect a ferrous−oxy complex, even on the stopped-flow time scale, is all the more surprising when one considers that human IDO has a similar reduction potential to rhTDO and forms a relatively stable ferrous−oxy intermediate (*6*). We were not able to assess whether binding of substrate to rhTDO stabilizes the ferrous−oxy complex (because this leads to turnover in the stopped-flow experiment), but the data that we have for binding of CO to rhTDO in the presence of substrate (which does not lead to turnover) do not support the idea that binding of L-Trp stabilizes the ferrous−oxy complex (data not shown).

Why is the ferrous−oxy complex of rhTDO so unstable? We do not have a complete answer at this stage, but we note that the S167H variant of rhIDO, in which an active site histidine, analogous to that presumed (from sequence alignments) to be present in rhTDO, has been incorporated, also has a very unstable ferrous−oxy complex (*6*).

Summary. Our data for rhTDO reveal several unexpected differences with other heme dioxygenases. (i) The catalytic ferrous−oxy complex of rhTDO is not detected at all even though the reduction potential for rhTDO is in a similar range to that for rhIDO in which the same complex is stable. This instability of the ferrous−oxy complex is not, however, reflected in the overall activity of the enzyme, which is on a par with other dioxygenases. (ii) rhTDO does not specifically favor substrate binding to the ferrous enzyme, as observed in other heme dioxygenases. (iii) The ferric form of rhTDO is also active toward substrate under aerobic conditions.

Collectively, what these data tell us is that, unlike other categories of heme proteins (e.g., peroxidases, globins) which have fairly consistent patterns of behavior, significant differences in mechanism and functional properties are already emerging across the heme dioxygenase family. The reasons for this remain to be established.

ACKNOWLEDGMENT

Peptide mass fingerprinting was carried out by Dr. Andrew R. Bottrill and Shairbanu Ibrahim from the Protein Nucleic Acid Chemistry Laboratory (PNACL), University of Leicester. We thank Dr. Harriet Seward for helpful discussions on EPR data.

SUPPORTING INFORMATION AVAILABLE

Amino acid sequence of rhTDO showing the peptides observed by MALDI-ToF after tryptic digest of rhTDO. This material is available free of charge via the Internet at http://pubs.acs.org.

REFERENCES

1. Sono, M., Roach, M. P., Coulter, E. D., and Dawson, J. H. (1996) Heme-containing dioxygenases. *Chem. Rev. 96*, 2841–2888.
2. Littlejohn, T. K., Takikawa, O., Skylas, D., Jamie, J. F., Walker, M. J., and Truscott, R. J. (2000) Expression and purification of recombinant human indoleamine 2,3-dioxygenase. *Protein Expression Purif. 19*, 22–29.
3. Papadopoulou, N. D., Mewies, M., McLean, K. J., Seward, H. E., Svistunenko, D. A., Munro, A. W., and Raven, E. L. (2005) Redox and spectroscopic properties of human indoleamine 2,3-dioxygenase and a His303Ala variant: implications for catalysis. *Biochemistry 44*, 14318–14328.
4. Vottero, E., Balgi, A., Woods, K., Tugendreich, S., Melese, T., Andersen, R. J., Mauk, A. G., and Roberge, M. (2006) Inhibitors of human indoleamine 2,3-dioxygenase identified with a target-based screen in yeast. *Biotechnol. J. 1*, 282–288.
5. Sugimoto, H., Oda, S., Otsuki, T., Hino, T., Yoshida, T., and Shiro, Y. (2006) Crystal structure of human indoleamine 2,3-dioxygenase: catalytic mechanism of O2 incorporation by a heme-containing dioxygenase. *Proc. Natl. Acad. Sci. U.S.A. 103*, 2611–2616.
6. Chauhan, N., Basran, J., Efimov, I., Svistunenko, D. A., Seward, H. E., Moody, P. C. E., and Raven, E. L. (2008) The role of serine 167 in human indoleamine 2,3-dioxygenase: a comparison with tryptophan 2,3-dioxygenase. *Biochemistry 47*, 4761–4769.
7. Antonini, M., and Brunori, E. (1971) *Hemoglobin and Myoglobin and their Reactions with Ligands*, North Holland Publishers, Amsterdam.
8. Leatherbarrow, R. J. (2001) Grafit version 5, Erithacus Software Ltd., Staines, U.K.
9. Patel, N., Jones, D. K., and Raven, E. L. (2000) Investigation of the haem-nicotinate interaction in leghaemoglobin. Role of hydrogen bonding. *Eur. J. Biochem. 267*, 2581–2587.
10. Speicher, K. D., Kolbas, O., Harper, S., and Speicher, D. W. (2000) Systematic Analysis of Peptide Recoveries from In-Gel Digestions for Protein Identifications in Proteome Studies. *J. Biomol. Technol. 11*, 74–86.
11. Massey, V. (1991) *Flavins and Flavoproteins* (Curti, B., Ronchi, S., and Zanetti, G., Eds.) pp 59–66, Walter de Gruyter, New York.
12. Clark, W. M. (1972) *Oxidation-Reduction Potentials of Organic Systems*, Kreiger Publishing, Huntington, NY.
13. Ren, S., Liu, H., Licad, E., and Correia, M. A. (1996) Expression of rat liver tryptophan 2,3-dioxygenase in *Escherichia coli*: structural and functional characterization of the purified enzyme. *Arch. Biochem. Biophys. 333*, 96–102.
14. Ishimura, Y., Nozaki, M., and Hayaishi, O. (1970) The oxygenated form of L-tryptophan 2,3-dioxygenase as reaction intermediate. *J. Biol. Chem. 245*, 3593–3602.
15. Manandhar, S. P., Shimada, H., Nagano, S., Egawa, T., and Ishimura, Y. (2002) Subunit structure of recombinant rat liver L-tryptophan 2,3-dioxygenase. *Int. Congr. Ser. 1233*, 161–169.
16. Matsumura, M., Osada, K., and Aiba, S. (1984) L-tryptophan 2,3-dioxygenase of a moderate thermophile, *Bacillus brevis*. Purification, properties and a substrate-mediated stabilization of the quaternary structure. *Biochim. Biophys. Acta 786*, 9–17.
17. Batabyal, D., and Yeh, S.-R. (2007) Human Tryptophan Dioxygenase: A Comparison to Indoleamine 2,3-Dioxygenase. *J. Am. Chem. Soc. 129*, 15690–15701.
18. Littlejohn, T. K., Takikawa, O., Truscott, R. J., and Walker, M. J. (2003) Asp274 and his346 are essential for heme binding and catalytic function of human indoleamine 2,3-dioxygenase. *J. Biol. Chem. 278*, 29525–29531.
19. Kudo, Y., and Boyd, C. A. R. (2000) Human placental indoleamine 2,3-dioxygenase: cellular localization and characterization of an enzyme preventing fetal rejection. *Biochim. Biophys. Acta 1500*, 119–124.
20. Watanabe, Y., Fujiwara, M., Yoshida, R., and Hayaishi, O. (1980) Stereospecificity of hepatic L-tryptophan 2,3-dioxygenase. *Biochem. J. 189*, 393–405.
21. Forouhar, F., Anderson, J. L., Mowat, C. G., Vorobiev, S. M., Hussain, A., Abashidze, M., Bruckmann, C., Thackray, S. J., Seetharaman, J., Tucker, T., Xiao, R., Ma, L. C., Zhao, L., Acton, T. B., Montelione, G. T., Chapman, S. K., and Tong, L. (2007) Molecular insights into substrate recognition and catalysis by tryptophan 2,3-dioxygenase. *Proc. Natl. Acad. Sci. U.S.A. 104*, 473–478.
22. Leeds, J. M., Brown, P. J., McGeehan, G. M., Brown, F. K., and Wiseman, J. S. (1993) Isotope effects and alternative substrate reactivities for tryptophan 2,3-dioxygenase. *J. Biol. Chem. 268*, 17781–17786.
23. Makino, R., Sakaguchi, K., Iizuka, T., and Ishimura, Y. (1980) Acid-alkaline transition and thermal spin equilibrium of the heme in ferric L-tryptophan 2,3-dioxygenases. *J. Biol. Chem. 255*, 11883–11891.
24. Makino, R., Sakaguchi, K., Iizuka, T., and Ishimura Y. (1980) L-Tryptophan 2,3-dioxygenase; structure, function an interaction with substrate, in *Biochemical and Medical Aspects of Tryptophan Metabolism* (Hayaishi, O., Ishimura, Y., and Kido, R., Eds.) pp 179–187, Elsevier/North Holland Biomedical Press, Amsterdam.
25. Hitchcock, M. J., and Katz, E. (1988) Purification and characterization of tryptophan dioxygenase from *Streptomyces parvulus*. *Arch. Biochem. Biophys. 261*, 148–160.
26. Zhang, Y., Kang, S. A., Mukherjee, T., Bale, S., Crane, B. R., Begley, T. P., and Ealick, S. E. (2007) Crystal structure and mechanism of tryptophan 2,3-dioxygenase, a heme enzyme involved in tryptophan catabolism and in quinolinate biosynthesis. *Biochemistry 46*, 145–155.

BI702393B